

## A 2D quantum dot array in planar $^{28}\text{Si}/\text{SiGe}$

Unsel, F. K.; Meyer, M.; Mażzik, M. T.; Borsoi, F.; de Snoo, S. L.; Amitonov, S. V.; Sammak, A.; Scappucci, G.; Veldhorst, M.; Vandersypen, L. M.K.

**DOI**

[10.1063/5.0160847](https://doi.org/10.1063/5.0160847)

**Publication date**

2023

**Document Version**

Final published version

**Published in**

Applied Physics Letters

**Citation (APA)**

Unsel, F. K., Meyer, M., Mażzik, M. T., Borsoi, F., de Snoo, S. L., Amitonov, S. V., Sammak, A., Scappucci, G., Veldhorst, M., & Vandersypen, L. M. K. (2023). A 2D quantum dot array in planar  $^{28}\text{Si}/\text{SiGe}$ . *Applied Physics Letters*, 123(8), Article 084002. <https://doi.org/10.1063/5.0160847>

**Important note**

To cite this publication, please use the final published version (if applicable).  
Please check the document version above.

**Copyright**

Other than for strictly personal use, it is not permitted to download, forward or distribute the text or part of it, without the consent of the author(s) and/or copyright holder(s), unless the work is under an open content license such as Creative Commons.

**Takedown policy**

Please contact us and provide details if you believe this document breaches copyrights.  
We will remove access to the work immediately and investigate your claim.

RESEARCH ARTICLE | AUGUST 22 2023

# A 2D quantum dot array in planar <sup>28</sup>Si/SiGe <sup>EP</sup>

F. K. Unseld <sup>ID</sup> ; M. Meyer <sup>ID</sup> ; M. T. Mađzik <sup>ID</sup> ; F. Borsoi <sup>ID</sup> ; S. L. de Snoo <sup>ID</sup> ; S. V. Amitonov <sup>ID</sup> ;  
A. Sammak <sup>ID</sup> ; G. Scappucci <sup>ID</sup> ; M. Veldhorst <sup>ID</sup> ; L. M. K. Vandersypen <sup>✉</sup> <sup>ID</sup>

 Check for updates

*Appl. Phys. Lett.* 123, 084002 (2023)

<https://doi.org/10.1063/5.0160847>

  
View  
Online

  
Export  
Citation

CrossMark

## Articles You May Be Interested In

On-chip integration of Si/SiGe-based quantum dots and switched-capacitor circuits

*Appl. Phys. Lett.* (October 2020)

Density dependence of the excitation gaps in an undoped Si/SiGe double-quantum-well heterostructure

*Appl. Phys. Lett.* (November 2021)

Germanium wafers for strained quantum wells with low disorder

*Appl. Phys. Lett.* (August 2023)

### 500 kHz or 8.5 GHz? And all the ranges in between.

Lock-in Amplifiers for your periodic signal measurements



Find out more

 Zurich  
Instruments

# A 2D quantum dot array in planar $^{28}\text{Si}/\text{SiGe}$ EP

Cite as: Appl. Phys. Lett. **123**, 084002 (2023); doi: 10.1063/5.0160847

Submitted: 6 June 2023 · Accepted: 29 July 2023 ·

Published Online: 22 August 2023



View Online



Export Citation



CrossMark

F. K. Unseld,<sup>1</sup> M. Meyer,<sup>1</sup> M. T. Mądzik,<sup>1</sup> F. Borsoi,<sup>1</sup> S. L. de Snoo,<sup>1</sup> S. V. Amitonov,<sup>1,2</sup> A. Sammak,<sup>2</sup> G. Scappucci,<sup>1</sup> M. Veldhorst,<sup>1</sup> and L. M. K. Vandersypen<sup>1,a)</sup>

## AFFILIATIONS

<sup>1</sup>QuTech and Kavli Institute of Nanoscience, Delft University of Technology, Lorentzweg 1, 2628 CJ Delft, The Netherlands

<sup>2</sup>QuTech and Netherlands Organization for Applied Scientific Research (TNO), Stieltjesweg 1, 2628 CK Delft, The Netherlands

<sup>a)</sup> Author to whom correspondence should be addressed: [l.m.k.vandersypen@tudelft.nl](mailto:l.m.k.vandersypen@tudelft.nl)

## ABSTRACT

Semiconductor spin qubits have gained increasing attention as a possible platform to host a fault-tolerant quantum computer. First demonstrations of spin qubit arrays have been shown in a wide variety of semiconductor materials. The highest performance for spin qubit logic has been realized in silicon, but scaling silicon quantum dot arrays in two dimensions has proven to be challenging. By taking advantage of high-quality heterostructures and carefully designed gate patterns, we are able to form a tunnel coupled  $2 \times 2$  quantum dot array in a  $^{28}\text{Si}/\text{SiGe}$  heterostructure. We are able to load a single electron in all four quantum dots, thus reaching the (1,1,1,1) charge state. Furthermore, we characterize and control the tunnel coupling between all pairs of dots by measuring polarization lines over a wide range of barrier gate voltages. Tunnel couplings can be tuned from about  $30 \mu\text{eV}$  up to approximately  $400 \mu\text{eV}$ . These experiments provide insightful information on how to design 2D quantum dot arrays and constitute a first step toward the operation of spin qubits in  $^{28}\text{Si}/\text{SiGe}$  quantum dots in two dimensions.

© 2023 Author(s). All article content, except where otherwise noted, is licensed under a Creative Commons Attribution (CC BY) license (<http://creativecommons.org/licenses/by/4.0/>). <https://doi.org/10.1063/5.0160847>

Since the original proposal for quantum computation with semiconductor quantum dots,<sup>1</sup> remarkable developments have been made. Quantum dot qubits are small in size, compatible with semiconductor manufacturing, and can be operated with single-qubit gate fidelities and two-qubit gate fidelities above 99.9%<sup>2</sup> and 99%,<sup>3–5</sup> respectively.

The implementation of two-dimensional qubit arrays will allow this technology platform to fully utilize its advantages. In GaAs heterostructures  $2 \times 2$  and  $3 \times 3$  quantum dot arrays have already been demonstrated.<sup>6–8</sup> However, hyperfine interaction leads to short dephasing times, preventing high-fidelity operation of qubit arrays. In contrast, group IV materials benefit from nuclear spin-free isotopes, such that quantum coherence can be maintained over much longer times.<sup>9</sup>

In recent years, hole quantum dots in Ge/SiGe heterostructures progressed from a single quantum dot to a  $4 \times 4$  quantum dot array with shared gate control.<sup>10–12</sup> Parallel to that also silicon based devices have been pushed toward 2D arrays. Using quantum dots confined in the corners of silicon nanowires, several  $2 \times N$  quantum dot arrays have been demonstrated, albeit not simultaneously at the single-electron occupancy.<sup>13–15</sup> Furthermore, these devices did not contain separate gates for independent control of the tunnel barriers between neighboring dots. This limits the controllability for quantum simulations and prevents sweet-spot operation<sup>16–18</sup> of exchange-based quantum gates.

In this work, we present a 2D quantum dot array in gated planar  $^{28}\text{Si}/\text{SiGe}$  with barrier gates to control inter-dot tunnel couplings. Four quantum dots in a  $2 \times 2$  configuration are formed with occupations controlled down to the last electron. Furthermore, all inter-dot tunnel couplings are characterized as a function of all barrier gate voltages. We demonstrate control over a wide range of tunnel couplings and provide suggestions for future scalable gate designs.

The  $2 \times 2$  quantum dot array investigated in this work is fabricated on a  $^{28}\text{Si}/\text{Si}_{70}\text{Ge}_{30}$  heterostructure (see the supplementary material). Figure 1(a) shows a false-colored scanning electron micrograph (SEM) image of a nominally identical device, highlighting the three gate layers of the multi-layer gate stack.<sup>19</sup> The screening gates in the first layer (purple) define an active area, reduce the formation of spurious dots, and prohibit accumulation of a two-dimensional electron gas (2DEG) in the gate fan-out region. The second layer (yellow) consists of plunger (P) and accumulation gates. Barrier gates (B) are fabricated in the third layer (red). On top of the gate stack sits a micro magnet. The SEM image in Fig. 1(a) is taken before its deposition to highlight the quantum dot gate pattern.

The gate stack defines four quantum dots in a  $2 \times 2$  grid (labeled clockwise 1–4) and two single-electron transistors (SETs) (S1 and S2). Gate and dot pitches were loosely adopted from the linear six dot array by Philips *et al.*<sup>20</sup> The screening gates around the four quantum dots

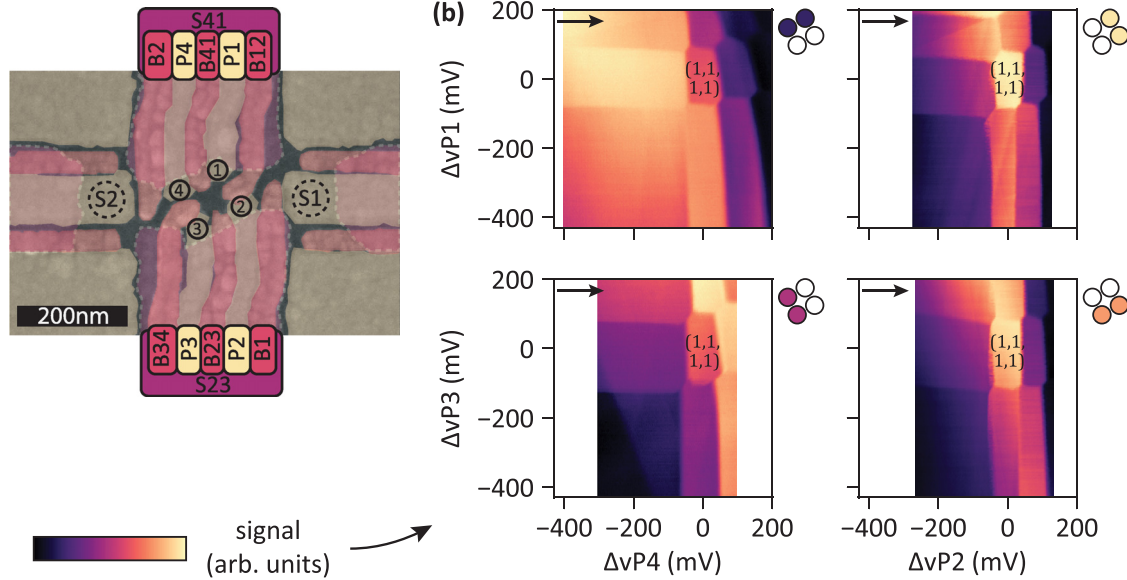


**FIG. 1.** (a) False colored SEM image of a nominally identical device to the one used in the measurements. The four quantum dots in the center are labeled clockwise 1–4 with one sensor on each side marked as S1 and S2. White dashed lines mark the boundaries of the screening gates in the first gate layer. (b) Charge stability diagrams of nearest-neighbor quantum dots. Colored circles indicate the quantum dots of the swept virtual plunger gates while the quantum dots corresponding to the white circles remained with one electron each. The point (0 mV, 0 mV) corresponds to the same gate voltages for all four scans. At this operating point, the (1,1,1,1) charge state is reached, with one electron per quantum dot. For the charge stability diagrams of Q1Q2 and Q2Q3, sensor S1 was used while for Q3Q4 and Q4Q1, sensor S2 was chosen. At  $\Delta vP_i = 0$  mV, the corresponding physical voltages on the gates are set to 2566, 1831, 3173, and 2487 mV for plungers 1–4, respectively. The arrows in the top left corner of each charge stability diagram indicate the direction of the scans.

were kept grounded. Two SETs serve as charge detectors and act as electron reservoirs for the quantum dots Q2 and Q4 in the  $2 \times 2$  array. Quantum dots Q1 and Q3 are loaded via Q2 and Q4, respectively. The presented data were taken exclusively with the sensor providing the highest contrast on the chosen dot pair for each measurement.

The  $22.5^\circ$  rotation of the square array relative to the micromagnets gives every quantum dot a distinct Zeeman splitting. The relative arrangement of the quantum dots and the SETs allows for sensing charge movements between all possible dot pairs. This is favorable for recording charge polarization lines and spin-to-charge conversion.

Off-chip NbTiN inductors connected to the SET reservoirs and parasitic capacitances form a tank circuit that enables radio frequency (RF) reflectometry readout, allowing for fast and accurate detection of the charge occupation of all four quantum dots.

During the device tune-up, we measure the cross-capacitive coupling of all gates to all dots and virtualize them as described in Ref. 21 with  $vP_i$  ( $vB_{ij}$ ) denoting the virtualized plunger (barrier) gates. The chosen virtual gates compensate the crosstalk onto all dot potentials and maintain the operation point of the charge sensors. The cross-capacitive coupling matrix  $\vec{M}$ , translating the real gate space to the virtual gate space via  $\vec{V}^{\text{virt}} = \vec{M}\vec{V}^{\text{real}}$ , is provided in the supplementary material.

To show control over the charge occupation of the entire  $2 \times 2$  array, we measure four charge stability diagrams, as depicted in Fig. 1(b). We acquire these data by sweeping the voltages on adjacent virtual plunger gates  $vP_i$  and  $vP_{(i \bmod 4)+1}$  while monitoring the response of the charge sensors. The colored circles in the top right corner of each charge stability diagram indicate the position of the quantum dots corresponding to the swept plunger gates.

A honeycomb pattern characteristic of double-dot behavior is observed for all four plunger pairs. We identify the first electron in the four quantum dots by the absence of any more charge transitions in the lower left corner. Thus, we can controllably access the  $(N_1, N_2, N_3, N_4) = (1, 1, 1, 1)$  charge state, where  $N_i$  denotes the charge occupation of quantum dot  $QD_i$ . Moreover, we can isolate a single spin per quantum dot. The honeycomb patterns in Fig. 1(b) also show that all four quantum dots are capacitively coupled to each other.

We note that there are apparent differences in the separation between the consecutive charge transition lines as well as in the slopes of successive charge transition lines. These could be caused by inherent differences and gate-voltage dependent variations in size, position, or lever arm of the four intended quantum dots. Alternatively, they might be the charging signature of additional quantum dots in the close vicinity. While we cannot fully rule out the presence of such stray dots at higher occupations, we can reliably reach the (1,1,1,1) charge state in the  $2 \times 2$  configuration of the array.

Next to the expected charge transitions, we observe additional diagonal features e.g., in Fig. 1(b), which we associate with spurious defects in our system. These defects capacitively couple to the charge sensor, but there is no or only very weak capacitive interaction with the four intentional quantum dots of the  $2 \times 2$  array.

In addition to a well-defined charge state, controlled inter-dot tunnel couplings are essential for the implementation of robust exchange-based quantum gates or the execution of analog quantum simulation. Therefore, we probe the system evolution as a function of the voltage applied to the virtual barrier gates  $vB_{ij}$  located between the

plunger gates of quantum dot  $QD_i$  and  $QD_j$  with  $j = (i \bmod 4) + 1$ . The tunnel coupling diagonally between  $QD_1$  and  $QD_3$  and anti-diagonally between  $QD_2$  and  $QD_4$  has no dedicated barrier gate and, thus, is not independently controllable. The influence of other barrier gates on the (anti-)diagonal tunnel coupling is presented below.

Figure 2 shows the evolution of the charge stability diagram of  $QD_2$  and  $QD_3$  while changing the virtual barrier gate voltage  $vB_{23}$ . The sequence of panels allows us to qualitatively assess the influence of the barrier on the capacitive coupling and tunnel coupling between the involved quantum dots. From panels I through IV, we observe that the separation between the triple points increases, which indicates an increase in the capacitive coupling between the dots. In addition, we observe that the interdot charge transition is increasingly blurred (see the circled transitions), and the boundaries of the charge stability diagram are increasingly rounded. Both are indicative of an increased interdot tunnel coupling. In panel IV, for transition lines with  $N_2 + N_3 \geq 4$ , the rounding is so strong that the quantum dots have mostly merged into a single large quantum dot.

To quantitatively determine the effect of the barrier voltage on the tunnel coupling, we measure polarization lines along the detuning axis  $\varepsilon_{ij}/\alpha_{vij} = vP_i - vP_j$ , with  $\alpha_{vij}$  denoting the lever arm, across the  $(N_i, N_j) = (1, 0)$  to  $(0, 1)$  interdot transition, as shown in Fig. 3(a). The remaining dots were kept in the  $(1,1)$  charge occupation. Scanning along this detuning axis moves the electron from dot 2 to dot 3 ( $(N_1, N_2, N_3, N_4) = (1, 1, 0, 1)$  to  $(1, 0, 1, 1)$ ), resulting in a step response in the sensor signal as seen in Fig. 3(b). This step response is broadened by both the electron temperature  $T_e \leq 78.5 \pm 2.2$  mK and the tunnel coupling  $t$  and can be fitted using  $S_{\text{sig}} = \frac{\varepsilon}{\Omega} \tanh \frac{\Omega}{2k_B T_e}$  with  $\Omega = \sqrt{\varepsilon^2 + 4t^2}$  and  $\varepsilon$  is the detuning between the two quantum dots.<sup>22</sup> Additional slopes and offsets of the sensor signal caused by imperfect virtualization or drifts are taken into account in the used fitting procedure.<sup>23</sup> We note that the error in the extracted tunnel coupling values is dominated by the uncertainty in the lever arms.

We systematically extract the dependency of the inter-dot tunnel couplings  $t_{n,m}$  between all dot pairs  $(QD_n, QD_m)$  with respect to all barrier voltages  $vB_{ij}$ . Figure 3(c) shows the resulting tunnel couplings  $t_{n,m}$  grouped by barrier gates  $vB_{ij}$ . As in previous works, fading contrast along the polarization lines prevented us from characterizing tunnel couplings up to higher values. We observe that changing the

barrier voltage  $vB_{ij}$  affects only the corresponding tunnel couplings  $t_{ij}$  significantly, while keeping the other tunnel couplings largely constant. Note that the virtual gate matrix compensates for crosstalk of the barrier gates onto all dot potentials but does not account for possible crosstalk on the tunnel couplings.

We, furthermore, find that below a given voltage (which is different for each  $vB_{ij}$ ), the influence of the barrier gate voltage on the corresponding tunnel coupling vanishes and a residual tunnel coupling remains. Across all four neighboring dot pairs, the residual tunnel coupling is in the range between 30 and 200  $\mu\text{eV}$ .

We extend this characterization to the (anti-)diagonal tunnel couplings. Figure 3(d) presents the influence of the four barrier gates on the diagonal and anti-diagonal tunnel coupling, respectively. While the anti-diagonal tunnel coupling  $t_{2,4}$  is elevated and can be modulated using  $vB_{12}$  in particular, the diagonal tunnel coupling  $t_{1,3}$  is not systematically influenced by any barrier gate and remains in many cases lower than all other tunnel couplings, albeit far from zero.

We demonstrated the first 2D quantum dot array in a planar silicon technology and operated the four quantum dots in the single electron regime, consistently achieving the  $(1, 1, 1, 1)$  charge state. Furthermore, the barrier gates allow us to independently control the interdot tunnel couplings. However, the residual tunnel couplings observed in this sample are higher than the typical tunnel couplings of 1–10  $\mu\text{eV}$  used in spin qubit experiments.<sup>24</sup> Presumably, the close proximity of the screening gates to the center of the plunger gates compresses the quantum dots toward the center of the  $2 \times 2$  array and hence toward each other, leading to rather large tunnel couplings. Furthermore, we see in Fig. 3 that at low tunnel coupling values, the tunnel coupling barely responds to the barrier gate voltages anymore. The compressed position of the quantum dots in the center region enhances also the diagonal coupling between them. While analog quantum simulation and quantum computation can benefit from diagonal tunnel coupling, the lack of dedicated control over magnitude and directionality i.e., diagonal vs anti-diagonal, also poses limitations. Suppressing any diagonal coupling with a center gate as demonstrated in a GaAs  $2 \times 2$  array could be a suitable way to circumvent this issue.<sup>25</sup>

The encountered challenges help to identify possible improvements in the design of planar  $2 \times 2$   $^{28}\text{Si}/\text{SiGe}$  quantum dot arrays. Specifically, moving the screening gates away from the center of the

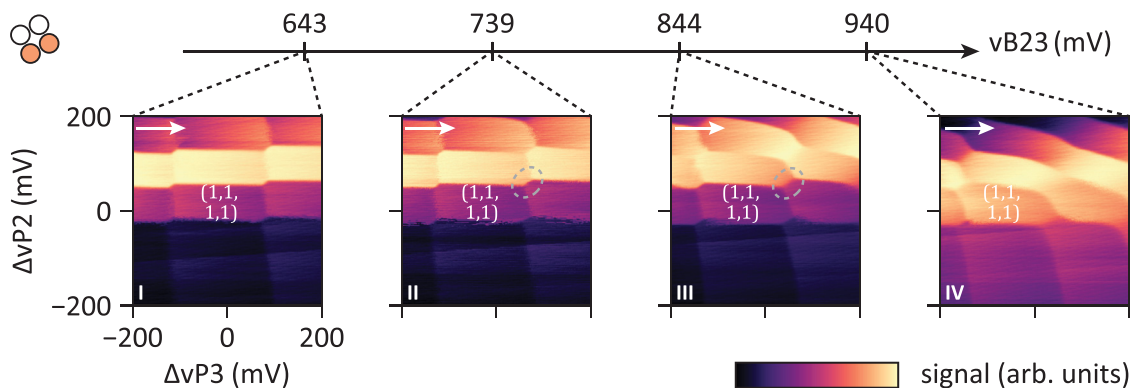
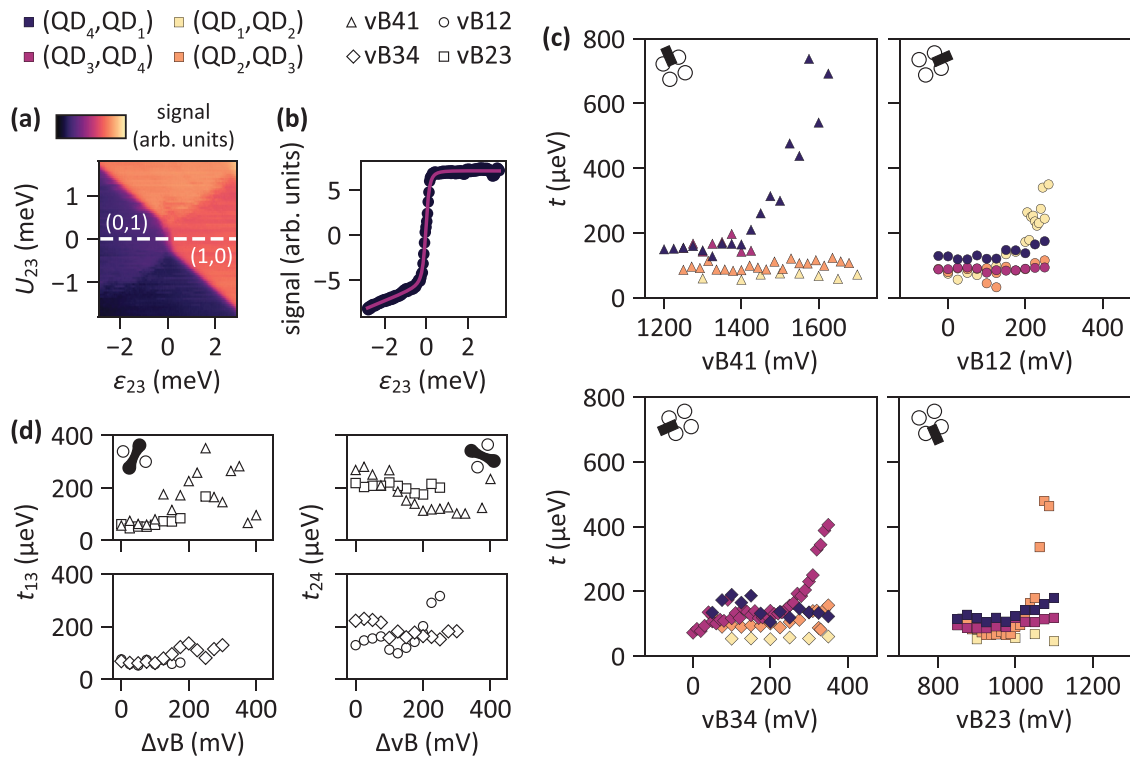


FIG. 2. Response of the charge stability diagram of  $QD_2$  and  $QD_3$  to changes of virtual barrier voltage  $vB_{23}$ , as indicated by the arrow above the charge stability diagrams. Small arrows in the top left corner of each panel indicate the scan direction. From panel I to IV, we observe a gradual increase in both the capacitive and tunnel coupling between the two dots. Similar data are taken for all other nearest-neighboring pairs and are displayed in the supplementary material.



**FIG. 3.** (a) Exemplary charge stability diagram around the (1,0) to (0,1) transition for QD<sub>2</sub> and QD<sub>3</sub> as a function of the interdot detuning  $\epsilon_{23}$  and  $U_{23}/\alpha_{U_{23}} = vP_2 + vP_3$ . The dashed line indicates the detuning axis used to measure polarization lines. (b) Example of a measured (dots) and fitted (solid line) polarization line for QD<sub>2</sub> and QD<sub>3</sub>. (c) Dependence of the tunnel couplings extracted from polarization lines between neighboring quantum dots on each of the four virtual barrier gate voltages. The plots are ordered to follow the physical position of the barrier gate, e.g., barrier  $vB_{41}$  situated in the top left corner of the quantum dot array is depicted in the top left plot. The legend for symbols and colors is shown above panels (a) and (b). We note that the dc voltages of barriers  $vB_{12}$  ( $vB_{23}$ ) and  $vB_{34}$  ( $vB_{41}$ ) are of comparable values, which is consistent with the symmetries of the gate pattern. Between scans, we adjusted gate voltages of uninvolved gates to retain a high visibility. These adjustments were done in such a way that all uninvolved barrier gates remained in the small (residual) tunnel coupling regime. On several occasions, insufficient contrast between the (1,0) and (0,1) charge states limited the data we were able to reliably fit. These data points are, thus, not available. (d) Diagonal tunnel coupling and anti-diagonal tunnel coupling as a function of all four virtual barrier gate voltages. The panels were split into two parts for both the diagonal and anti-diagonal coupling to keep the data points visible. The physical gate voltages used at  $\Delta vB = 0$  mV varies between datasets, as the voltages were slightly adjusted. As in (c) uninvolved barrier gates remained in the residual tunnel coupling regime. Note also that in (c) and (d) the charge states vary between scans, depending on which dots each polarization line connects.

array is expected to yield lower tunnel couplings, as the electrons are not squeezed toward each other as much. The experiments also offer relevant learnings for scaling to larger arrays. For instance, changing the device architecture from a square array to a triangular array will alleviate the issues regarding undesired diagonal tunnel couplings.<sup>26,27</sup> Furthermore, in order to maintain control of individual tunnel couplings, either more sophisticated patterning techniques must be applied to route gates to the inside of a larger array<sup>28</sup> or crossbar addressing must be employed.<sup>12,29,30</sup> In both cases, the observations made for the present device provide guidance for suitable plunger and barrier gate pitches and dimensions.

See the supplementary material for details on the device fabrication and screening, the experimental setup and the virtual gate matrix of Fig. 1; the extension to Fig. 2, the response of all four charge stability diagrams to potential changes on the corresponding barrier; and the methodology of how the lever arms and the electron temperature were extracted.

We acknowledge the funding by Intel Corporation and fruitful discussions provided by everyone in the Veldhorst Lab and Vandersypen Lab.

## AUTHOR DECLARATIONS

### Conflict of Interest

The authors have no conflicts to disclose.

### Author Contributions

Florian K. Unsel and Marcel Meyer contributed equally to this work.

**Florian K. Unsel:** Conceptualization (lead); Data curation (equal); Formal analysis (equal); Investigation (lead); Methodology (equal); Resources (equal); Validation (equal); Visualization (equal); Writing – original draft (lead); Writing – review & editing (lead). **Marcel Meyer:** Conceptualization (lead); Data curation (lead); Formal analysis (lead);

Investigation (lead); Methodology (equal); Validation (equal); Visualization (lead); Writing – original draft (equal); Writing – review & editing (equal). **Mateusz T. Mađzik**: Formal analysis (supporting); Investigation (supporting); Supervision (supporting); Validation (supporting); Writing – review & editing (supporting). **Francesco Borsoi**: Formal analysis (supporting); Investigation (supporting); Methodology (supporting); Software (equal); Validation (supporting); Writing – review & editing (supporting). **Sander L. de Snoo**: Software (lead); Writing – review & editing (supporting). **Sergey V. Amitonov**: Resources (equal); Writing – review & editing (supporting). **Amir Sammak**: Resources (equal); Writing – review & editing (supporting). **Giordano Scappucci**: Resources (equal); Writing – review & editing (supporting). **Menno Veldhorst**: Conceptualization (lead); Funding acquisition (lead); Project administration (lead); Supervision (lead); Validation (equal); Writing – review & editing (equal). **Lieven M. K. Vandersypen**: Conceptualization (lead); Funding acquisition (lead); Project administration (lead); Supervision (lead); Validation (equal); Writing – review & editing (lead).

## DATA AVAILABILITY

The data and analysis scripts that support the findings of this study are openly available in the Zenodo repository at <https://doi.org/10.5281/zenodo.7957630> (Ref. 31).

## REFERENCES

- <sup>1</sup>D. Loss and D. P. DiVincenzo, “Quantum computation with quantum dots,” *Phys. Rev. A* **57**, 120–126 (1998).
- <sup>2</sup>J. Yoneda, K. Takeda, T. Otsuka, T. Nakajima, M. R. Delbecq, G. Allison, T. Honda, T. Kodera, S. Oda, Y. Hoshi, N. Usami, K. M. Itoh, and S. Tarucha, “A quantum-dot spin qubit with coherence limited by charge noise and fidelity higher than 99.9%,” *Nat. Nanotechnol.* **13**, 102–106 (2018).
- <sup>3</sup>X. Xue, M. Russ, N. Samkharadze, B. Undseth, A. Sammak, G. Scappucci, and L. M. K. Vandersypen, “Quantum logic with spin qubits crossing the surface code threshold,” *Nature* **601**, 343–347 (2022).
- <sup>4</sup>A. Noiri, K. Takeda, T. Nakajima, T. Kobayashi, A. Sammak, G. Scappucci, and S. Tarucha, “Fast universal quantum gate above the fault-tolerance threshold in silicon,” *Nature* **601**, 338–342 (2022).
- <sup>5</sup>A. R. Mills, C. R. Guinn, M. J. Gullans, A. J. Sigillito, M. M. Feldman, E. Nielsen, and J. R. Petta, “Two-qubit silicon quantum processor with operation fidelity exceeding 99%,” *Sci. Adv.* **8**, eabn5130 (2022).
- <sup>6</sup>J. P. Dehollain, U. Mukhopadhyay, V. P. Michal, Y. Wang, B. Wunsch, C. Reichl, W. Wegscheider, M. S. Rudner, E. Demler, and L. M. K. Vandersypen, “Nagaoka ferromagnetism observed in a quantum dot plaquette,” *Nature* **579**, 528–533 (2020).
- <sup>7</sup>P.-A. Mortemousque, B. Jadot, E. Chanrion, V. Thiney, C. Bäuerle, A. Ludwig, A. D. Wieck, M. Urdampilleta, and T. Meunier, “Enhanced spin coherence while displacing electron in a two-dimensional array of quantum dots,” *PRX Quantum* **2**, 030331 (2021).
- <sup>8</sup>F. Fedele, A. Chatterjee, S. Fallahi, G. C. Gardner, M. J. Manfra, and F. Kuemmeth, “Simultaneous operations in a two-dimensional array of singlet-triplet qubits,” *PRX Quantum* **2**, 040306 (2021).
- <sup>9</sup>P. Stano and D. Loss, “Review of performance metrics of spin qubits in gated semiconducting nanostructures,” *Nat. Rev. Phys.* **4**, 672–688 (2022).
- <sup>10</sup>N. W. Hendrickx, W. I. L. Lawrie, M. Russ, F. van Riggelen, S. L. de Snoo, R. N. Schouten, A. Sammak, G. Scappucci, and M. Veldhorst, “A four-qubit germanium quantum processor,” *Nature* **591**, 580–585 (2021).
- <sup>11</sup>F. van Riggelen, W. I. L. Lawrie, M. Russ, N. W. Hendrickx, A. Sammak, M. Rispler, B. M. Terhal, G. Scappucci, and M. Veldhorst, “Phase flip code with semiconductor spin qubits,” *npj Quantum Inf.* **8**, 124 (2022).
- <sup>12</sup>F. Borsoi, N. W. Hendrickx, V. John, S. Motz, F. van Riggelen, A. Sammak, S. L. de Snoo, G. Scappucci, and M. Veldhorst, “Shared control of a 16 semiconductor quantum dot crossbar array,” [arXiv:2209.06609](https://arxiv.org/abs/2209.06609) (2022).
- <sup>13</sup>W. Gilbert, A. Saraiva, W. H. Lim, C. H. Yang, A. Laucht, B. Bertrand, N. Rambal, L. Hutin, C. C. Escott, M. Vinet, and A. S. Dzurak, “Single-electron operation of a silicon-CMOS  $2 \times 2$  quantum dot array with integrated charge sensing,” *Nano Lett.* **20**, 7882–7888 (2020).
- <sup>14</sup>E. Chanrion, D. J. Niegemann, B. Bertrand, C. Spence, B. Jadot, J. Li, P.-A. Mortemousque, L. Hutin, R. Maurand, X. Jehl, M. Sanquer, S. D. Franceschi, C. Bäuerle, F. Balestro, Y.-M. Niquet, M. Vinet, T. Meunier, and M. Urdampilleta, “Charge detection in an array of CMOS quantum dots,” *Phys. Rev. Appl.* **14**, 024066 (2020).
- <sup>15</sup>F. Ansaloni, H. Bohuslavskiy, F. Fedele, T. Rasmussen, B. Brovang, F. Berritta, A. Heskies, J. Li, L. Hutin, B. Venitucci, B. Bertrand, M. Vinet, Y.-M. Niquet, A. Chatterjee, and F. Kuemmeth, “Gate reflectometry in dense quantum dot arrays,” *New J. Phys.* **25**, 033023 (2023).
- <sup>16</sup>F. Martins, F. K. Malinowski, P. D. Nissen, E. Barnes, S. Fallahi, G. C. Gardner, M. J. Manfra, C. M. Marcus, and F. Kuemmeth, “Noise suppression using symmetric exchange gates in spin qubits,” *Phys. Rev. Lett.* **116**, 116801 (2016).
- <sup>17</sup>M. Reed, B. Maune, R. Andrews, M. Borselli, K. Eng, M. Jura, A. Kiselev, T. Ladd, S. Merkel, I. Milosavljevic, E. Pritchett, M. Rakher, R. Ross, A. Schmitz, A. Smith, J. Wright, M. Gyure, and A. Hunter, “Reduced sensitivity to charge noise in semiconductor spin qubits via symmetric operation,” *Phys. Rev. Lett.* **116**, 110402 (2016).
- <sup>18</sup>B. Bertrand, H. Flentje, S. Takada, M. Yamamoto, S. Tarucha, A. Ludwig, A. D. Wieck, C. Bäuerle, and T. Meunier, “Quantum manipulation of two-electron spin states in isolated double quantum dots,” *Phys. Rev. Lett.* **115**, 096801 (2015).
- <sup>19</sup>W. I. L. Lawrie, H. G. J. Eenink, N. W. Hendrickx, J. M. Boter, L. Petit, S. V. Amitonov, M. Lodari, B. P. Wuetz, C. Volk, S. G. J. Philips, G. Droulers, N. Kalhor, F. van Riggelen, D. Brousse, A. Sammak, L. M. K. Vandersypen, G. Scappucci, and M. Veldhorst, “Quantum dot arrays in silicon and germanium,” *Appl. Phys. Lett.* **116**, 080501 (2020).
- <sup>20</sup>S. G. J. Philips, M. T. Mađzik, S. V. Amitonov, S. L. de Snoo, M. Russ, N. Kalhor, C. Volk, W. I. L. Lawrie, D. Brousse, L. Tryptuten, B. P. Wuetz, A. Sammak, M. Veldhorst, G. Scappucci, and L. M. K. Vandersypen, “Universal control of a six-qubit quantum processor in silicon,” *Nature* **609**, 919–924 (2022).
- <sup>21</sup>C. Volk, A. M. J. Zwerver, U. Mukhopadhyay, P. T. Eendebak, C. J. van Diepen, J. P. Dehollain, T. Hensgens, T. Fujita, C. Reichl, W. Wegscheider, and L. M. K. Vandersypen, “Loading a quantum-dot based ‘Qubyte’ register,” *npj Quantum Inf.* **5**, 29 (2019).
- <sup>22</sup>L. DiCarlo, H. J. Lynch, A. C. Johnson, L. I. Childress, K. Crockett, C. M. Marcus, M. P. Hanson, and A. C. Gossard, “Differential charge sensing and charge delocalization in a tunable double quantum dot,” *Phys. Rev. Lett.* **92**, 226801 (2004).
- <sup>23</sup>C. J. van Diepen, P. T. Eendebak, B. T. Buijtenorp, U. Mukhopadhyay, T. Fujita, C. Reichl, W. Wegscheider, and L. M. K. Vandersypen, “Automated tuning of inter-dot tunnel coupling in double quantum dots,” *Appl. Phys. Lett.* **113**, 033101 (2018).
- <sup>24</sup>T. J. Knapp, R. T. Mohr, Y. S. Li, B. Thorgrimsson, R. H. Foote, X. Wu, D. R. Ward, D. E. Savage, M. G. Lagally, M. Friesen, S. N. Coppersmith, and M. A. Eriksson, “Characterization of a gate-defined double quantum dot in a Si/SiGe nanomembrane,” *Nanotechnology* **27**, 154002 (2016).
- <sup>25</sup>U. Mukhopadhyay, J. P. Dehollain, C. Reichl, W. Wegscheider, and L. M. K. Vandersypen, “A  $2 \times 2$  quantum dot array with controllable inter-dot tunnel couplings,” *Appl. Phys. Lett.* **112**, 183505 (2018).
- <sup>26</sup>A. Noiri, K. Kawasaki, T. Otsuka, T. Nakajima, J. Yoneda, S. Amaha, M. R. Delbecq, K. Takeda, G. Allison, A. Ludwig, A. D. Wieck, and S. Tarucha, “A triangular triple quantum dot with tunable tunnel couplings,” *Semicond. Sci. Technol.* **32**, 084004 (2017).
- <sup>27</sup>H. Flentje, P.-A. Mortemousque, R. Thalineau, A. Ludwig, A. D. Wieck, C. Bäuerle, and T. Meunier, “Coherent long-distance displacement of individual electron spins,” *Nat. Commun.* **8**, 501 (2017).
- <sup>28</sup>W. Ha, S. D. Ha, M. D. Choi, Y. Tang, A. E. Schmitz, M. P. Levendorf, K. Lee, J. M. Chappell, T. S. Adams, D. R. Hulbert, E. Acuna, R. S. Noah, J. W. Matten, M. P. Jura, J. A. Wright, M. T. Rakher, and M. G. Borselli, “A flexible design

- platform for Si/SiGe exchange-only qubits with low disorder,” *Nano Lett.* **22**, 1443–1448 (2022).
- <sup>29</sup>M. Veldhorst, H. G. J. Eenink, C. H. Yang, and A. S. Dzurak, “Silicon CMOS architecture for a spin-based quantum computer,” *Nat. Commun.* **8**, 1766 (2017).
- <sup>30</sup>R. Li, L. Petit, D. P. Franke, J. P. Dehollain, J. Helsen, M. Steudtner, N. K. Thomas, Z. R. Yoscovits, K. J. Singh, S. Wehner, L. M. K. Vandersypen, J. S. Clarke, and M. Veldhorst, “A crossbar network for silicon quantum dot qubits,” *Sci. Adv.* **4**, eaar3960 (2018).
- <sup>31</sup>F. K. Unseld, M. Meyer, M. Madzik, F. Borsoi, S. de Snoo, S. Amitonov, A. Sammak, G. Scappucci, M. Veldhorst, and L. Vandersypen (2023). “Dataset underlying the manuscript: A 2D quantum dot array in planar  $^{28}\text{Si}/\text{SiGe}$ ,” Zenodo. <https://doi.org/10.5281/zenodo.7957630>